

Conductivity-depth imaging of time-domain EM data based on pseudo-layer half-space model

Haoping Huang, *Geo-EM, LLC., Raleigh, NC, USA*

Jonathan Rudd*, *Aeroquest, Ltd., Milton, ON, Canada*

Summary

A conductivity depth imaging (CDI) algorithm for concentric-coil helicopter time-domain electromagnetic (HTEM) systems is developed based on the pseudo-layer half-space model. The primary advantages of this model are immunity to altimeter errors, and a bias towards conductive layers. Effective depth is derived empirically from the computed conductivity, sampling time, and apparent thickness of the pseudo-layer. A table lookup procedure is created based on the analytic solution to the half-space models to speed up the processing. This efficiency makes the generation of real-time CDIs possible. Tests of the program on synthetic and field data yield stable and geologically meaningful results.

Introduction

Helicopter-borne time-domain electromagnetic (EM) systems with a concentric coil configuration are well-established in mineral exploration. Conductivity depth imaging (CDI) has been proven to be a useful tool in mapping the distribution of geologic conductivity and for identifying conductive sources within a variably conductive host geology. There are a number of methods for deriving fast conductivity-depth sections from time-domain EM data. One group of the methods is based on the Maxwell receding image concept, where conductivity is derived from a predicted depth for an image source (e.g., Macnae and Lamontagne, 1987). Approximate imaging schemes based on the actual depth of the maximum current or the maximum sensitivity to a layer in a half-space have also been developed (e.g., Eaton and Hohmann, 1989; Fullagar, 1989). Another approach is to transform the time-domain EM data to time-constant space (Macnae et al., 1998). The thin-sheet approach developed for time-domain data has also been used to generate CDI's (Macnae et al., 1991; Tartaras et al., 2000). A modification of this method was introduced to add the possibility of recovering the magnetic properties of the geology (Zhdanov and Pavlov, 2001). Still further development of this technique involved the application of the localized S-inversion (Zhdanov et al., 2002).

In this paper, we present an approach to CDI using a pseudo-layer half-space model originally developed by Fraser (1978) for frequency-domain helicopter EM systems. The concept of effective depth is used in this original work. The new algorithm as applied to time-domain data is tested on synthetic and field data with encouraging results.

AeroTEM systems

The original concept of a coincident coil helicopter-borne time domain system was pioneered by Aerodat scientists in the early 1980's under the guidance of Wally Bokyo. Aeroquest has since refined the system design into an effective and field-worthy exploration tool that is optimized to provide the maximum amount of information on a target conductor. The transmitter waveform is a bipolar triangular pulse which can be operated at 30, 90 and 150 Hz. The vertical and horizontal components of the secondary magnetic fields are measured during both the transmitter on-time and off-time. The diameter of transmitter loop varies from system to system from 5 m to 12 m. The strengths of the AeroTEM systems include high spatial resolution, broadband response, source geometry discrimination, and depth penetration.

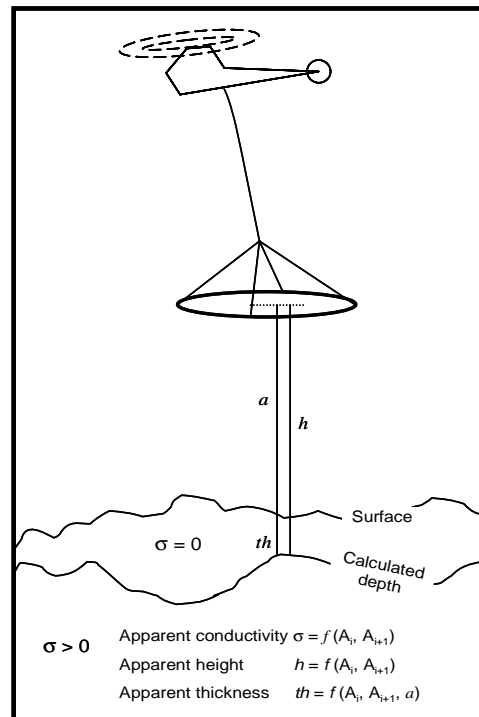


Figure 1: The system and pseudo-layer half-space model.

Conductivity Depth Imaging of time-domain HTEM data based on the pseudo-layer model

Method

The system and model are shown in Figure 1. The pseudo-layer half-space model is equivalent to a two-layer case where the upper layer is of zero conductivity. Its thickness th is the difference between the interpreted height h and the bird altitude a as obtained from the altimeter. The upper layer of the pseudo-layer half-space model is merely an artifice to account for the difference between the computed sensor-source height h and the measured sensor altitude a . The measured sensor altitude is determined from the altimeter. Any error in the altimeter reading, e.g., as caused by a forest canopy, falls into the computed sensor-source height and therefore does not corrupt the computed conductivity. The pseudo-layer half-space is the model of choice for displaying the apparent conductivity in both plan and section, in part because of this immunity to altimeter errors (Fraser, 1978; Huang and Fraser, 1996). The other advantage of this model is that the resulting conductivity biases to conductive targets, allowing us to recognize bedrock conductors easier than the homogeneous half-space model (Fraser, 1978).

For concentric transmitting and receiving coils, the half-space response in the frequency domain can be found in Ward and Hohmann (1988). The frequency-domain response can then be transformed to the time-domain using fast Fourier transformation. Figure 2 depicts the off-time response, A , to a half-space as a function of conductivity σ . The response for each channel, given in nT/s, increases with increasing conductivity at low conductivities, reaches a peak at moderate conductivity (about 1 S/m), and then decreases as σ continues to increase.

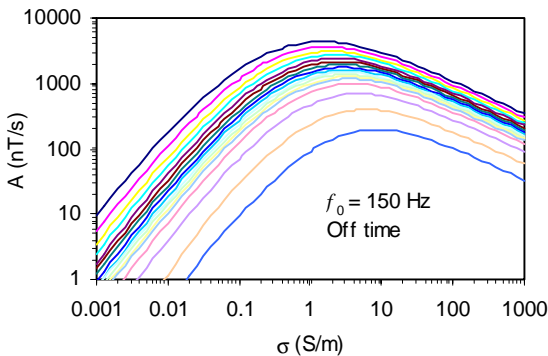


Figure 2: Response to a homogeneous half-space at a bird height of 30 m.

We can see from Figure 2 that conductivity cannot be uniquely determined from a single channel of data, but that it can be derived from any two channels. The time constant, τ_i , and amplitude β_i can be calculated from any two channels as,

$$\tau_i = \frac{t_{i+k} - t_i}{\ln\left(\frac{A_i}{A_{i+k}}\right)}, \text{ and} \quad (1)$$

$$\beta_i = (A_i^2 + A_{i+k}^2)^{1/2}, \quad (2)$$

where t_i and A_i are the center time and the measured amplitude in nT/s at i -th channel, respectively. k is the channel interval used to calculate τ_i and β_i . Apparent conductivity σ_a and apparent bird height h can be computed from a pair of τ_i and β_i . The apparent thickness th of pseudo-layer can be calculated from h and measured bird altitude a , i.e., $th=h-a$. If there are N channels of data available, $N-k$ apparent conductivities and apparent thicknesses can be computed.

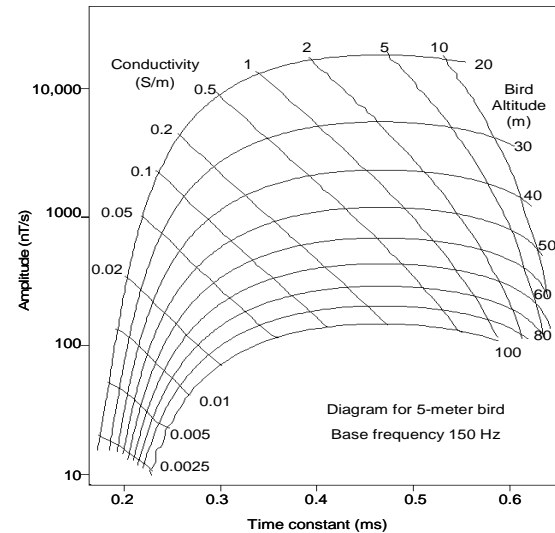


Figure 3: A diagram of time constant τ_i and amplitude β_i of half-space model for two time-off channels.

In practice, we create a lookup table to compute σ and h based on the analytic solutions in order to speed up the process. This procedure is easily understood by using a graphic presentation as shown in Figure 3. Here, a diagram is used to yield a unique σ and h from each pair of τ_i and β_i . For measured data, we can calculate the τ_i and β_i from any two channels. This pair is then located in one of the $N-k$ lookup tables to determine conductivity σ and height h . The solutions are interpolated where the location does not fall directly on the conductivity-altitude curves. If the earth is truly homogeneous, the conductivity obtained from Figure 3 is equal to the true conductivity σ . Where it is not

Conductivity Depth Imaging of time-domain HTEM data based on the pseudo-layer model

homogeneous, the solution is called an apparent conductivity σ_a .

An effective depth d_i associated with conductivity σ_i can be approximated from the conductivity σ_i , apparent thickness th_i and sampling time t_i . As we know, the effective depth is proportional to sampling time t_i and inversely proportional to conductivity σ_i . Thus, we write

$$\delta_i = \left(\frac{t_i}{\sigma_i \mu_0 \pi} \right)^{1/2}, \quad (3)$$

where μ_0 is the magnetic permeability of free space. Since the pseudo-layer model is used, the effective depth is related to the apparent thickness, and in general can be written as

$$d_i = f(\delta_i, th_i). \quad (4)$$

Figure 4 provides a graphic presentation of the effective depth as a function of δ_i and th_i . Since the effective depth is an empirical approach, Figure 4 should be viewed as the current manifestation of this parameter which, in the future, may be altered to yield an improved conductivity-depth section.

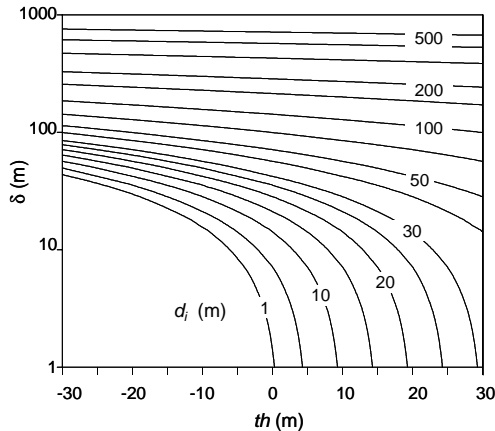


Figure 4: The effective depth as a function of δ and th .

The algorithm is tested on synthetic data. True conductivity and height are returned from data computed using a series of homogeneous half-space models. The errors in conductivity and height are generally less than 0.1%.

We then simulate a dipping thin conductive layer (200 mS/m) sandwiched in a resistive host (20 mS/m) by using a series of 3-layer models. As shown in Figure 5, the depth of the 20 m thick conductive layer increases from 50 m on the

left to 200m on the right. The color section represents the results from the algorithm. The resulting CDI image reasonably approximates the original dipping conductive layer indicated by the black lines.

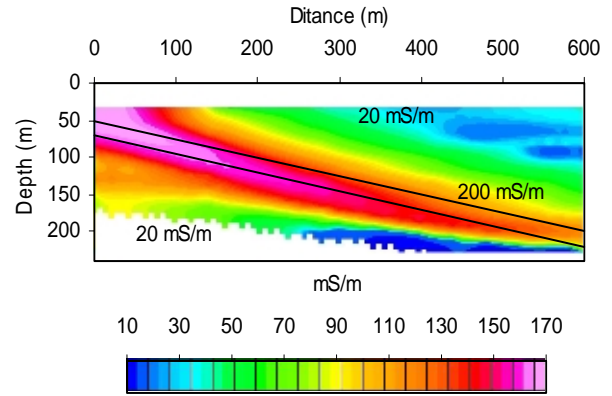


Figure 5: CDI results for a dipping thin (20 m) conductive layer of 200 mS/m in a resistive host of 20 mS/m.

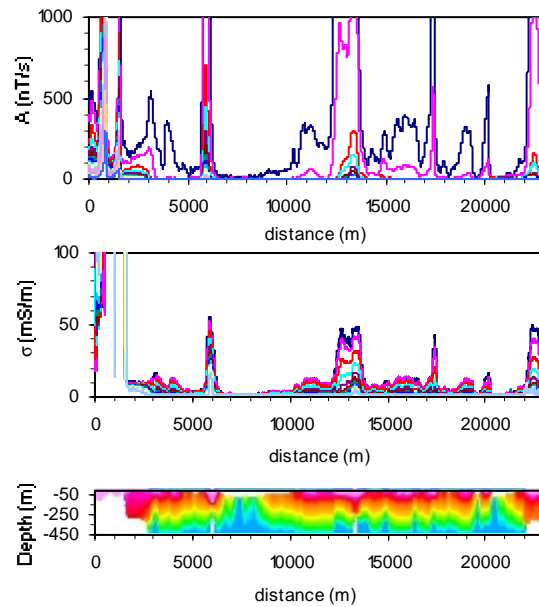


Figure 6: Off-time HTEM data, apparent conductivity profiles and section.

Field examples

Data for the first field example were collected in an area where a variable layer of conductive overburden occurs over a resistive geology. Figure 6 shows the off-time data from a long line (23-km), the computed apparent conductivity, and the resulting CDI section. Note that mush

Conductivity Depth Imaging of time-domain HTEM data based on the pseudo-layer model

of the line has a high amplitude rapidly decaying response typical of a conductive surface layer. This response is accurately modeled in the CDI as near-surface conductive layer. This dataset, which comprises over 10 thousand data points, took only a few seconds to process for the apparent conductivities and CDI.

The second field example is from a conductive area (see Figure 7). Two depth slice plan maps for depths of 80 m and 160 m and a CDI section crossing at $y=1650$ m are shown. Conductivity maps, which can be produced for any depth from the CDI results, are an effective way of visualizing conductive layers and features. A southeast trending conductive feature passing through $x=6830$ and $y=1500$ is very clear on the maps, and becomes stronger at depth. This feature is very difficult to identify in the raw data.

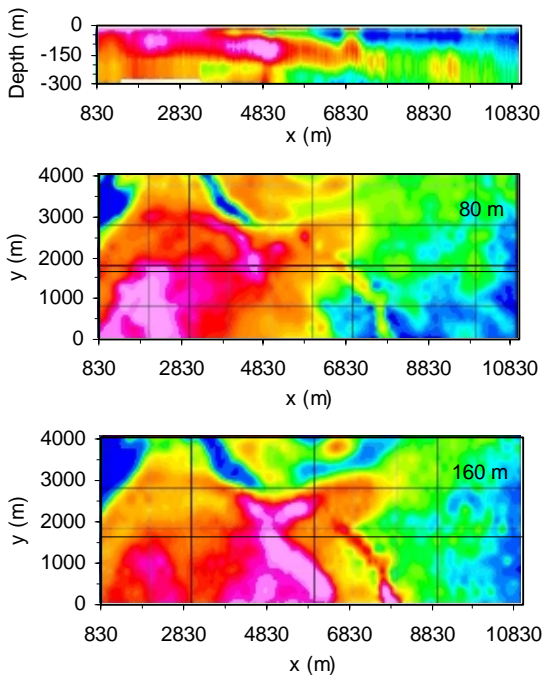


Figure 7: The CDI and two depth slices at 80 m and 160 m.

Conclusions

An algorithm is developed for computing the apparent conductivity and effective depth from concentric-coil helicopter time-domain data based on the pseudo-layer half-space model. Two advantages of this model are immunity to altimeter errors, and a bias to conductive layers. A table lookup procedure is created based on the analytic solution to the half-space model to speed up the processing and making real-time processing of CDIs

possible. Tests of the program on synthetic and field data yield stable and geologically meaningful results.

References

- Fraser, D. C., 1978, Resistivity mapping with an airborne multicoil electromagnetic system: *Geophysics*, **43**, 144-172.
- Fullagar, P., 1989, Generation of conductivity-depth pseudo-sections for coincident loop and in-loop TEM data: 7th Geophysical Conference, Austr. Soc. Expl. Geophys., **20**, 43-45.
- Huang, H., and Fraser, D.C., 1996, The differential parameter method for multifrequency airborne resistivity mapping: *Geophysics*, **61**, 100-109.
- Macnae, J.C., King, A., Stolz, N., Osmakoff, A., Blaha, A., 1998, Fast AEM data processing and inversion: *Exploration Geophysics*, **29**, 163-169.
- Macnae, J. C., Smith, R., Polzer, B. D., Lamontagne, Y. and Klinkert, P. S., 1991, Conductivity-depth imaging of airborne electromagnetic step-response data: *Geophysics*, **56**, 102-114.
- Tartaras, E., Zhdanov, M. S., Wada, K., Saito, A., and Hara, T., 2000, Fast imaging of TDEM data based on S-inversion: *Journal of Applied Geophysics*, **43**, No. 1, 15-32.
- Ward, S. H., and Hohmann, G. W., 1988, Electromagnetic theory for geophysical applications: in Nabighian, M. N., Ed., *Electromagnetic Methods in Applied Geophysics*, **1**, Theory, 130-311.
- Zhdanov, M. S., and Pavlov, D. A., 2001, Analysis and interpretation of anomalous conductivity and magnetic permeability effects in time domain electromagnetic data. Part II: $S\mu$ -inversion: *Journal of Applied Geophysics*, **46**, 4, 235-248.
- Zhdanov, M.S., Pavlov, D. A., and Ellis, R., 2002, Localized S-inversion of time domain electromagnetic data: *Geophysics*, **67**, No. 4, 1115-1125.

Acknowledgments

Haoping Huang gratefully acknowledges the support of this work by Aeroquest Limited. The authors would also like to thank Associated Mining Consultants Ltd. of Calgary, Alberta, for their valuable contributions to this paper.

EDITED REFERENCES

Note: This reference list is a copy-edited version of the reference list submitted by the author. Reference lists for the 2006 SEG Technical Program Expanded Abstracts have been copy edited so that references provided with the online metadata for each paper will achieve a high degree of linking to cited sources that appear on the Web.

REFERENCES

- Fraser, D. C., 1978, Resistivity mapping with an airborne multicoil electromagnetic system: *Geophysics*, **43**, 144–172.
- Fullagar, P., 1989, Generation of conductivity-depth pseudo-sections for coincident loop and in-loop TEM data: 7th Geophysical Conference, ASEG, **20**, 43–45.
- Huang, H., and D. C. Fraser, 1996, The differential parameter method for multifrequency airborne resistivity mapping: *Geophysics*, **61**, 100–109.
- Macnae, J. C., A. King, N. Stolz, A. Osmakoff, and A. Blaha, 1998, Fast AEM data processing and inversion: *Exploration Geophysics*, **29**, 163–169.
- Macnae, J. C., R. Smith, B. D. Polzer, Y. Lamontagne, and P. S. Klinkert, 1991, Conductivity-depth imaging of airborne electromagnetic step-response data: *Geophysics*, **56**, 102–114.
- Tartaras, E., M. S. Zhdanov, K. Wada, A., Saito, and T. Hara, 2000, Fast imaging of TDEM data based on S-inversion: *Journal of Applied Geophysics*, **43**, 15–32.
- Ward, S. H., and G. W. Hohmann, 1988, Electromagnetic theory for geophysical applications: *Electromagnetic Methods in Applied Geophysics*, **1**, 130–311.
- Zhdanov, M. S., and D. A. Pavlov, 2001, Analysis and interpretation of anomalous conductivity and magnetic permeability effects in time domain electromagnetic data. Part II: S_{μ} -inversion: *Journal of Applied Geophysics*, **46**, 235–248.
- Zhdanov, M. S., D. A. Pavlov, and R. Ellis, 2002, Localized S-inversion of time domain electromagnetic data: *Geophysics*, **67**, 1115–1125.